Sensors & Actuators: A. Physical 384 (2025) 116264

Contents lists available at ScienceDirect

Sensors and Actuators: A. Physical

journal homepage: www.journals.elsevier.com/sensors-and-actuators-a-physical

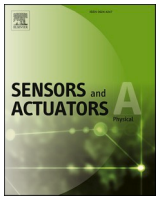

A flexible ultra-robust ZnO-AgNWs/PDMS-based hybrid nanogenerator for simultaneous energy harvesting and sensing applications

Wei Chen [a], Sheng-Zhe Zhao [a], Guo-Tao Xiang [a], Ran Lu [a], Jia-Lei Xu [a], Raul D. Rodriguez [b,*], Evgeniya Sheremet [b], Yong-Da Hu [c,*], Jin-Ju Chen [a,*]

[a] School of Materials and Energy, University of Electronic Science and Technology of China, Chengdu 610054, PR China
[b] Tomsk Polytechnic University, 30 Lenin Ave, Tomsk 634050, Russia
[c] School of Integrated Circuit Science and Engineering, University of Electronic Science and Technology of China, Chengdu 610054, PR China

ARTICLE INFO

Keywords:
Piezoelectric generator
PDMS-based
Energy harvesting
Self-powered
Wearable electronics sensors

ABSTRACT

Developing high-power output, flexible, and wearable electronics is a significant challenge to materials science. We address this issue by creating a hybrid piezo-triboelectric nanogenerator (PTNG) based on a unique combination of porous ZnO, silver nanowires (AgNWs), and polydimethylsiloxane (PDMS). Our PTNG utilizes porous ZnO, which exhibits a significantly higher piezoelectric coefficient than its non-porous counterpart due to its increased surface area and enhanced atomic polarization. This unique combination of porous ZnO, AgNWs, and PDMS creates a synergistic effect, enhancing both piezoelectric and triboelectric outputs beyond what each material could achieve alone. For instance, our device generates an open-circuit voltage of 146 V and a short-circuit current of 1.1 μA under a pressure of 12.5 kPa and can track human motion while generating 60 V during regular walking. Deformation tests show excellent performance with prolonged use for up to two months. This robust, flexible, and highly sensitive PTNG opens opportunities for next-generation self-powered wearable sensors and energy harvesting applications in healthcare, fitness, and other emerging technologies, particularly those already using PDMS as a base material.

1. Introduction

Developing light, robust, low-cost power sources is critical for safely developing and adopting wearable and flexible electronics. In this context, piezoelectric nanogenerators (PENGs) and triboelectric nanogenerators (TENGs) are promising as wearable power sources due to their portability and versatility [1–5]. TENGs perform well at low frequencies, while PENGs have rapid response, making them highly complementary in flexible self-powered sensing devices [6–10]. Although the mechanisms behind piezoelectric and triboelectric generators are different, there are some common characteristics in the mechanical-to-electrical energy conversion process without interfering with each other [11]. Thus, integrating these effects in piezoelectric and triboelectric nanogenerators (PTNGs) is being explored to harvest mechanical energy [12–15]. A critical challenge for wearable applications is achieving high piezo-triboelectric output while maintaining flexibility, biocompatibility, and adaptability [16]. The key to overcoming this issue is selecting suitable materials to obtain efficient PTNGs with high degrees of wearability and durability.

ZnO-based nanogenerators, which were first demonstrated in 2006, have shown great promise as energy-harvesting devices [17]. This is partly due to ZnO's remarkable piezoelectric coefficient, biocompatibility, and appearance in different nanostructure forms [18]. Among the various ZnO forms available most research has concentrated on 1D structures, such as nanowires, nanorods, and nanofibers [19–21]. Here, we focus on the untapped and relatively unexplored perspectives of microporous fibers, allowing us to investigate the potential of enhanced piezoelectric performance due to their larger surface area compared to non-porous nanostructures.

Investigating ZnO porous nanostructures adds to current strategies, like doping, surface and interface modification, and reducing the area density [22–28], developed to optimize the performance for piezoelectric device applications, for instance, by mitigating the effects of free charge carriers in n-type ZnO [29–32].

Polydimethylsiloxane (PDMS) polymers are widely used in wearable electronics as triboelectric materials due to their high electronegativity,

* Corresponding authors.
E-mail addresses: raul@tpu.ru (R. Lu), raul@tpu.ru (R.D. Rodriguez), yongnet169@uestc.edu.cn (Y.-D. Hu), jinjuchen@uestc.edu.cn (J.-J. Chen).

https://doi.org/10.1016/j.sna.2025.116264
Received 29 September 2024; Received in revised form 27 December 2024; Accepted 25 January 2025
Available online 30 January 2025

flexibility, and chemical stability. Improving TENGs' performance requires enhancing the surface charge density. This can be achieved by manipulating surface states and modifying the dielectric characteristics of the triboelectric materials [33,34]. Another point for improved performance in PENG applications is the internal resistance of the bulk materials, which can be reduced by introducing electrically conductive fillers [35–37]. Materials with high aspect ratios and conductivity, such as carbon nanotubes and silver nanowires (AgNWs), are promising candidates.

In this work, we introduce a rational design to create high-performance piezo-triboelectric hybrid nanogenerators combining porous ZnO as the piezoelectric material, AgNWs as the conductive filler, and PDMS as the triboelectric material and flexible matrix. We selected AgNWs instead of Ag nanoparticles because they offer superior electrical conductivity, a high aspect ratio, and enhanced mechanical strength and flexibility. These properties are crucial for creating efficient conductive pathways within the device and ensuring long-term stability. We systematically investigated the individual contributions of piezoelectricity and triboelectricity and optimized their integration for total output performance. Moreover, our devices demonstrate high sensitivity to different body motions and remarkable flexibility, reaching 300 % stretching and a range of deformations relevant to wearable applications. This research presents a promising strategy for developing efficient wearable energy harvesters from mechanical stimuli, offering a sustainable and reliable power source for various electronic devices and Internet-of-Things applications.

2. Results and discussion

Our ZnO-AgNWs/PDMS composite is illustrated by the sketch in Fig. 1a, showing the diverse components with SEM imaging results of the actual samples in Figs. 1b and 1c. The preparation process involving electrospinning to obtain ZnO and sintering at 700°C is illustrated in Figure S1 in the Supporting Information (SI). SEM results in Fig. 1b show that the ZnO fibers surface morphology has a unique porous structure that arises from polyvinylpyrrolidone (PVP) decomposition during the sintering process [38]. In contrast, commercial ZnO shows a rather dendritic-like morphology, as evidenced by SEM in Figure S2. Fig. 1c reveals the high aspect ratio and uniformity of the AgNWs, making them ideal for creating a highly conductive network. The cross-sectional morphology observed by SEM (Fig. 1d) shows close contact between the piezoelectric ZnO and triboelectric PDMS materials, with AgNWs sparsely distributed, forming a conductive framework. We expected that this conductive network could significantly enhance the efficiency of ZnO-AgNWs/PDMS-based piezo-triboelectric nanogenerators.

Energy-dispersive X-ray spectroscopy (EDS) elemental mapping

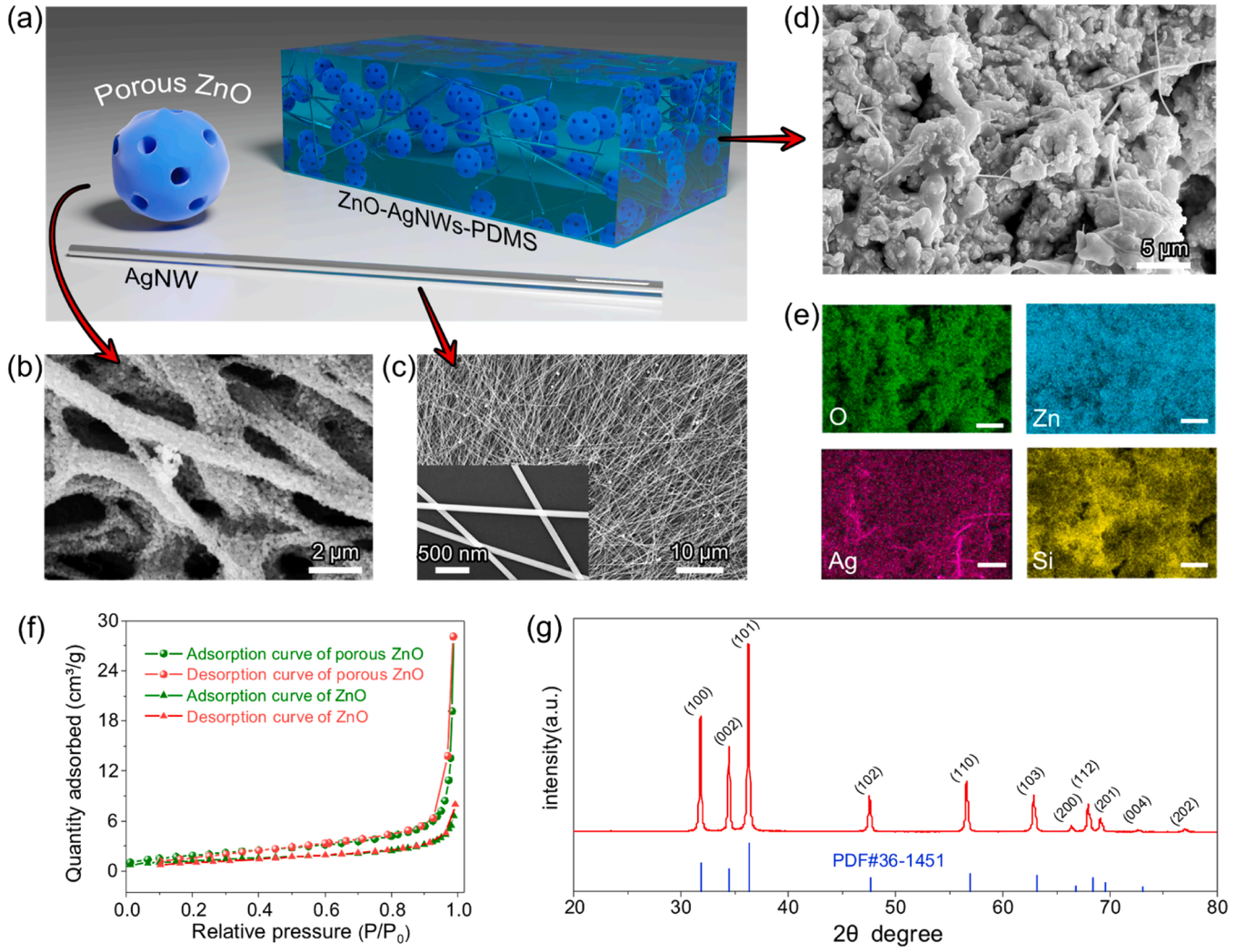

Fig. 1. (a) Schematic illustration of the ZnO-AgNWs/PDMS composite. The morphology is simplified to a porous sphere, highlighting the porous nature of ZnO. SEM images of (b) porous ZnO and (c) AgNWs. (d) Cross-sectional SEM image of the composite and (e) corresponding EDX mapping of the ZnO-AgNWs/PDMS composite; the scale bars are 5 μm. (f) N_2 adsorption/desorption isotherms for porous ZnO and commercial ZnO. (g) XRD spectrum of the as-prepared porous ZnO.

allowed us to determine the spatial distribution of the different elements making up our composite. The EDS maps (Fig. 1e) revealed a uniform distribution of oxygen, zinc, silver, and silicon throughout the composite. Comparing commercial to ZnO, Brunauer–Emmett–Teller (BET) analysis results in Fig. 1f, Figure S3, and Table S1 show a significant increase in surface area and micropore volume for our porous counterpart. We expected this since a larger pore volume and higher specific surface area provide a more favorable microstructure for deformation and piezoelectric performance. The X-ray diffraction (XRD) pattern in Fig. 1g was recorded from the synthesized ZnO, showing peaks in the 2θ range of 20°-80°. The diffraction peaks at 31.94°, 34.58°, 36.39°, 47.67°, and 56.78° correspond to the (100), (002), (101), (102), and (110) planes of wurtzite ZnO, respectively (JCPDS card no. 36–1451).

An interesting feature of our ZnO-AgNWs/PDMS device is that it combines triboelectric and piezoelectric effects for power generation. The specific power generation process depicted in Fig. 2a involves: 1) Initial state: no power generation due to the contact material and the PTNG separation; 2) Contact: establishment of equal amounts of opposite charges due to electron transfer between the contact material and the PTNG; 3) Separation: electron flow from the ground to the electrode to maintain charge neutrality, generating a triboelectric current (I_t); 4) Contact: electron flow back to the ground establishing a reverse

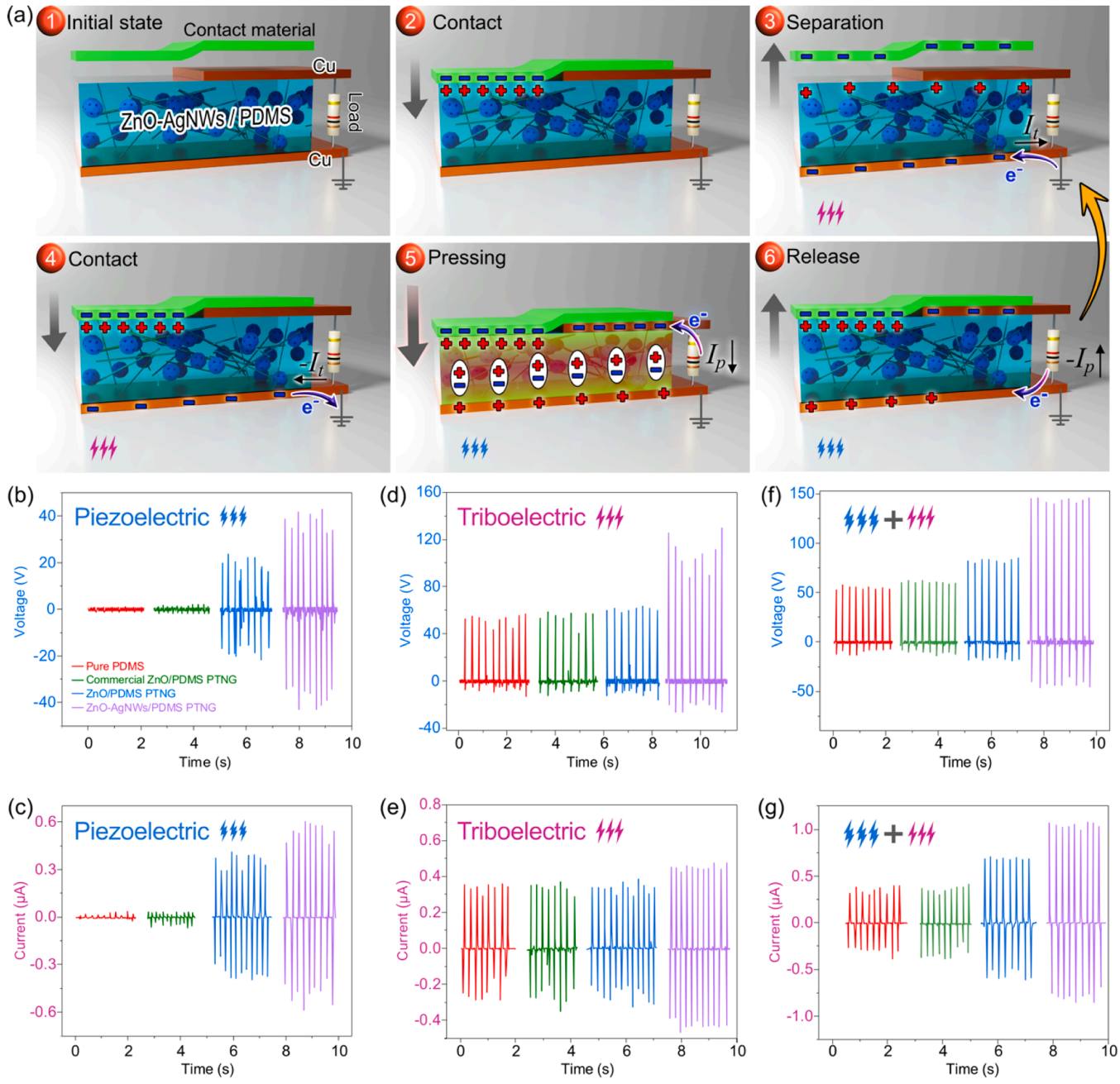

Fig. 2. (a) Key steps in ZnO-AgNWs/PDMS PTNG energy generation. 1) Initial state: The PTNG is in a neutral state with no contact with the contact material. 2) Contact: Charges accumulate at the interface after touching the contact material. 3) Separation: Charge imbalance occurs, inducing a triboelectric current (I_t). 4) Contact: Re-contact causes charges to redistribute, resulting in a reverse triboelectric current ($-I_t$). 5) Pressing: Mechanical pressure induces piezoelectric charge generation (I_p). 6) Release of pressure: Causes a redistribution of charges, creating a reverse piezoelectric current ($-I_p$). Electrical outputs: piezoelectric voltage (b) and current (c), triboelectric voltage (d) and current (e), and combined voltage (f) and current (g) signals for pure PDMS, commercial ZnO/PDMS PTNG, ZnO/PDMS PTNG, and ZnO-AgNWs/PDMS PTNG.

triboelectric current (-I_t); 5) Pressing: piezoelectric polarization of ZnO due to deformation by the external force resulting in an additional piezoelectric current (I_p); 6) Release: Removal of compressive strain and disappearance of piezoelectric polarization, leading to a reverse current (-I_p). After this separation step, the system goes back to step 3, completing the power generation cycle.

Since our ZnO-AgNWs/PDMS PTNG device was constructed with naturally flexible structures to harvest electricity from mechanical energy, we performed dedicated experiments to evaluate electrical performance given by voltage and current output. To quantitatively assess the relative piezoelectric and triboelectric contributions to the current and voltage outputs, we tested PTNG devices in piezoelectric, triboelectric, and hybrid modes. We performed this analysis for PTNGs made of pure PDMS, commercial ZnO/PDMS PTNG, ZnO/PDMS PTNG, and ZnO-AgNWs/PDMS. Figs. 2b and 2c show the results from this output comparison, revealing that the pure PDMS generator lacked piezoelectric output while the commercial ZnO device displayed only weak piezoelectricity. In contrast, the porous ZnO-based device exhibited high piezoelectric performance, with a piezoelectric output further enhanced after adding AgNWs. The piezoelectric coefficients of the commercial ZnO/PDMS composite and the porous ZnO/PDMS composite were measured to be approximately 5 pC/N and 27 pC/N, respectively. This indicates a significant enhancement in the piezoelectric response due to the introduction of porosity.

Herein, we also investigate the influence of AgNWs on the triboelectric output of ZnO/PDMS PTNGs. The triboelectric outputs of the four devices are compared in Figs. 2d and 2e. We see that the introduction of AgNWs significantly enhanced the piezoelectric output. At the same time, there was no significant change in the triboelectric response for the cases of pure PDMS generators, commercial ZnO/PDMS PTNG, and ZnO/PDMS PTNG. This observation suggests that the triboelectric signal mainly originates from PDMS, and it can be improved by introducing AgNWs as conductive fillers. The hybrid output performance of the four nanogenerators is shown in Fig. 2f and g. The ZnO-AgNWs/PDMS PTNG exhibits the highest performance with an open-circuit voltage of 146 V and a short-circuit current of 1.1 μA, which is significantly higher than any of the other devices.

To confirm the device's capacity to monitor diverse signals, the electrical outputs of the ZnO-AgNWs/PDMS PTNG were recorded under different loading frequencies in the 1–5 Hz range. Results in Figs. 3a and 3b show that the device can capture real-time electrical signals at those frequencies. Moreover, both voltage and current show an upward trend as the frequency increases, indicating the nanogenerator's capability to operate under various scenarios involving different frequencies. Furthermore, Fig. 3c shows the relative resistance changes (R/R_0) of the ZnO/PDMS and the ZnO-AgNWs/PDMS composite during stretching deformation. Remarkably, when the stretching reaches 300 %, the ZnO-AgNWs/PDMS composite exhibits a significantly lower resistance variation of 10^3 compared to the ZnO/PDMS composite. This enhanced electrical stability against deformation is attributed to the conductive network facilitated by the AgNWs. Consequently, the device's electrical pathway is less prone to mechanical fracture, essential for applications in wearable electronics requiring super-stretchability. It is important to note that the resistance variation measurement was conducted under tensile deformation, while the electrical output testing in Fig. 2 was performed under compressive pressure, resulting in different electrical responses.

We evaluated the power output performance of the ZnO-AgNWs/PDMS PTNG device by connecting in a series of different external load resistances ranging from 100 Ω to 1 GΩ. As evidenced by results in Fig. 3d, the short-circuit current decreased with the increase in resistance load, while the open-circuit voltage increased. The power density was calculated using the formula $P = U \times I/S$, where I and U represent the short-circuit current and open-circuit voltage under a specified external load resistance, respectively, and S is the effective contact area [39]. The maximum power density of 221.1 mW/m^2 (Fig. 3e) is obtained for an external load resistance of 2×10^7 Ω.

For practical applications in flexible and wearable devices, the energy harvester must have excellent robustness and stable long-term performance. Fig. 3f presents the critical durability characteristics of

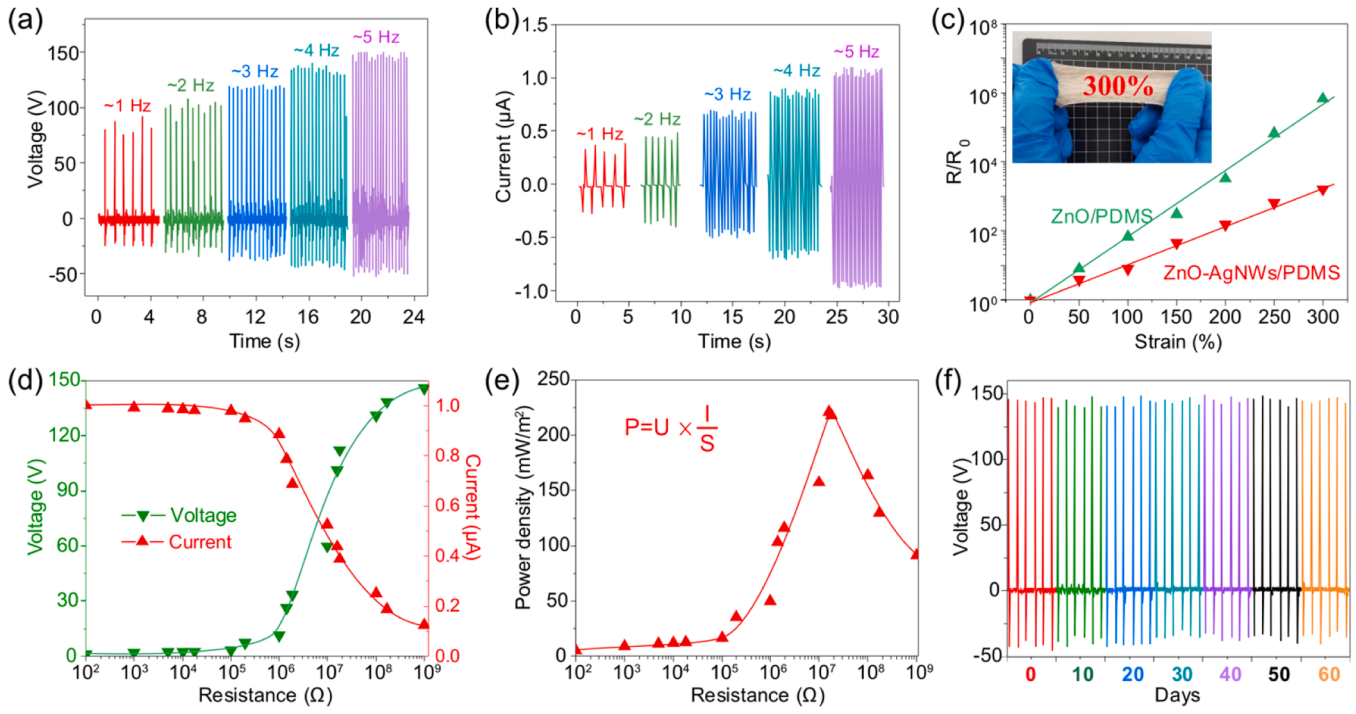

Fig. 3. Performance characteristics of the ZnO-AgNWs/PDMS nanogenerator. (a) Voltage and (b) current outputs at different frequencies from 1 Hz to 5 Hz. (c) Relative resistance change (R/R_0) as a function of strain. The inset shows 300 % stretchability. (d) Voltage and current as a function of resistance. (e) Power density calculated as $P = U \times I/S$ (power = voltage × current/area) against resistance. (f) Long-term stability test showing consistent voltage output over 60 days of cyclic loading.

the ZnO-AgNWs/PDMS PTNG recorded over a 60-days evaluation period. The output voltage signal remained stable throughout the period, demonstrating our PTNG device's long-term stability.

To further investigate the functionality and resilience of the PTNG device, we subjected it to different mechanical deformations, including twisting, bending, and stretching. The results in Fig. 4 and S4 show the remarkable mechanical resilience of our device that despite significant kinds and degrees of deformation, there were zero failures. The time-dependent output responses in Fig. 4 show that the device consistently produced voltage and current signals regardless of the deformation experienced. This capability highlights the potential of our PTNG as a robust energy harvester and motion sensor since it can capture and convert kinetic energy from various deformation-based activities into electrical signals, making it a prospective solution for real-time motion monitoring.

The performance comparison of our discovery versus the state-of-the-art has been made, as shown in Table 1. It can be clearly seen that our device exhibits a solid mechanical energy harvesting performance compared to other works, and in terms of sustainable performance, our PTNG has high stability and excellent flexibility. During 60 days of storage or 5000 cycles of compressive stress (Figure S5), the electrical output of the device remains almost unchanged, and it can sustain electrical output despite undergoing different mechanical deformations. The pressure sensitivity of the device is defined as the output voltage for applied pressure, and we further compare the present work with previous devices, as shown in Fig. 5a. It should be noted that the pressures in these works are at the same level. Obviously, the present device exhibits exceptional pressure sensitivity.

Now, we focus on evaluating the applicability of our ZnO-AgNWs/PDMS PTNG as a wearable power source and self-powered device. This evaluation was done by connecting the PTNG device to various electronic components, including a full-wave rectifier bridge, to form an energy rectification and storage circuit, as depicted in Figure S6a. Electric energy was continuously generated when pressure was repeatedly applied to the PTNG and then rectified by the bridge (Figure S6b). The charging capacity of the PTNG was evaluated using standard off-the-shelve capacitors. Results in Fig. 5b and Figure S7 demonstrate the PTNG's charging performance for multiple capacitors with an ultimate charging voltage reaching over 8 V for a 1 μF capacitor. This charge was sufficient to power multiple LEDs, as shown in Fig. 5c. Additionally, as evidenced in Fig. 5c and Video S1, the PTNG could directly power an LCD screen, demonstrating its potential for self-powered wearable electronics applications.

The human body is an intricate system with plenty of physical signals and untapped mechanical energy generated by relentless body motion. Harnessing these signals and energy is critical for monitoring exercise and fitness levels, sleep, and eating habits and ultimately achieving a more complete dataset for healthcare [48–50]. To address this need, our novel ZnO-AgNWs/PDMS material in a PTNG device combines energy harvesting with remarkable resilience against deformation and long-term performance. Moreover, this material's properties enable it to conform closely to different body parts, thanks to the PDMS matrix, allowing the recording of physiological signals during human movement and offering real-time, non-invasive monitoring. For instance, when attached to the human knees or elbows (Fig. 5d and e), our ZnO-AgNWs/PDMS PTNG generates consistent electrical signals as the legs or arms bend back and forth (see Video S2). The versatility of our generator is illustrated when attaching it to a shoe sole. During regular walking, the PTNG can produce a voltage of 60 V (Fig. 5f), demonstrating its effectiveness in harvesting mechanical energy that otherwise

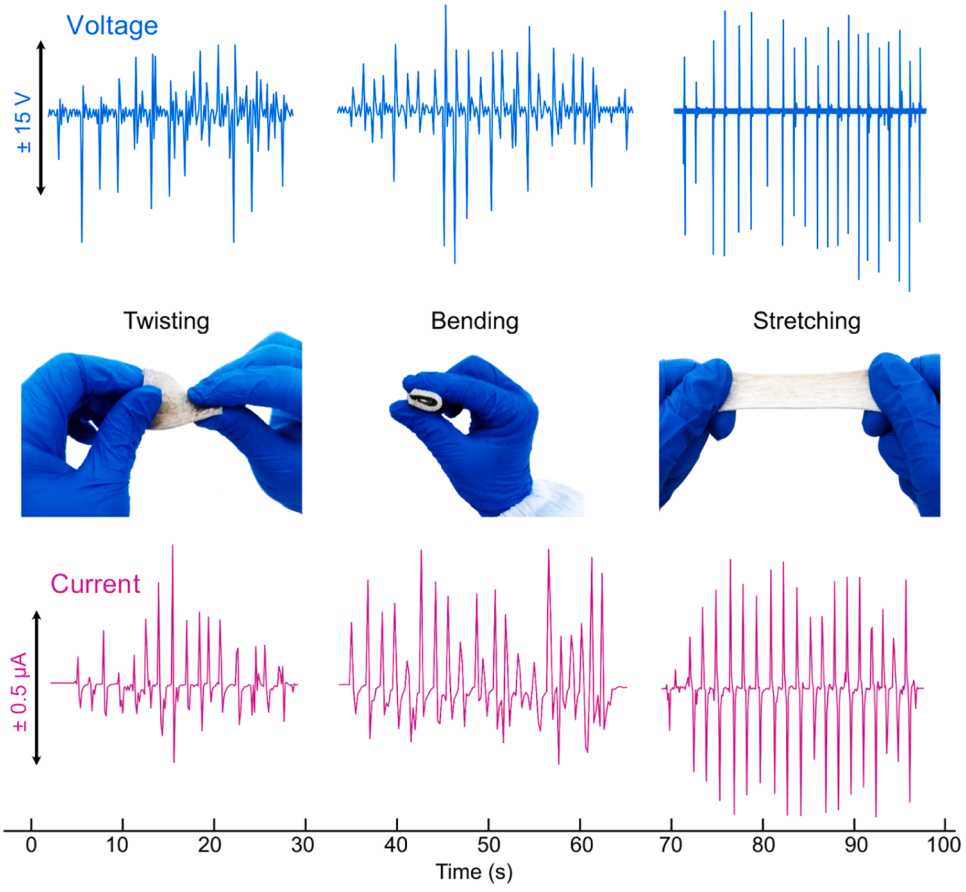

Fig. 4. Electrical output for different mechanical deformations. The data at the top row shows the voltage produced in our PTNG material when subjected to twisting, bending, and stretching, as shown by photographs in the middle row. The bottom row shows the respective current outputs for each deformation type.

Table 1
The performance comparison of our device with some state-of-the-art nanogenerators.

Materials	Dimensions	Force / Pressure	Frequency (Hz)	V_{OC} (V)	I_{SC} (μA)	Maximum power	Stability	Ref.
PVDF/MoS_2@ ZnO	2 × 3 cm^2	100 kPa	–	6.22	0.528	3.28 μW	–	[40]
MXene/PVDF	Round piece with 1.6 cm diameter	200 kPa	1.5	3.15	0.134	43.59 nW (89 kPa)	5000 cycles (64 kPa, 1 Hz)	[41]
PVDF/CNF@ ZnO	2.5 × 1.8 cm^2	45 N	2.5	11.8	0.452	5.26 μW	600 s	[42]
CNF@ZnO/ PDMS	2 × 2 cm^2	25 N	3	25.6	1.1	–	1500 cycles	[43]
PVDF/PDMS	1.33 × 1.33 cm^2	10 N	1	88	5.85	286 mW/m^2	5000 cycles	[44]
ZnO/Ag/PDMS	2 × 4 cm^2	10 N	3	20	0.2	6 μW/cm^2 (0.75 N, 20 Hz)	30000 cycles (0.75 N, 5 Hz)	[45]
PAN/$BaTiO_3$/ MXene	2 × 2 cm^2	30 N	1	11.3	0.3	3.4 mW/m^2	3000 cycles	[46]
ZnO–$ZnWO_4$@PDMS	1 × 4 cm^2	30 N	3	1.32	–	9.7 μW/m^2	30 days	[47]
ZnO-AgNWs/PDMS	**1 × 2 cm^2**	**12.5 kPa**	**5**	**146**	**1.1**	**221.1 mW/m^2**	**60 days 5000 cycles**	**This work**

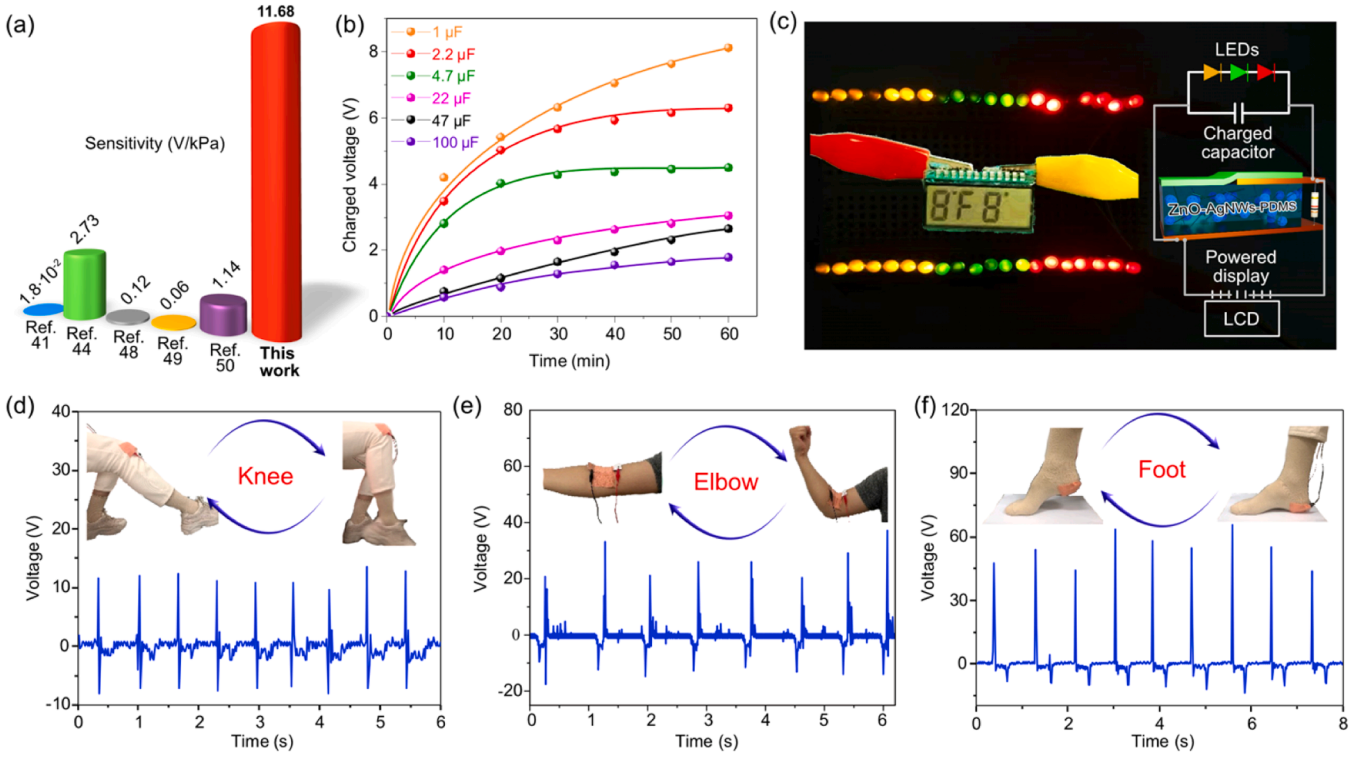

Fig. 5. (a) A comparison of the present work with previous devices on pressure sensitivity. (b) Voltage curves over time for various capacitors charged by the ZnO-AgNWs/PDMS nanogenerator. (c) Circuit of the nanogenerator charging a capacitor to power an array of LEDs and directly power an LCD. (d), (e), and (f) Voltage output generated by the PT NG attached to the knee, elbow, and foot, respectively. Each graph shows the electrical signals for different joint motions.

goes to waste.

We used Finite Element Simulations (FEM, COMSOL Multiphysics 5.6) to model ZnO with different numbers of micropores. This allowed us to study the effects of porous structure and specific surface area on piezoelectric output. The FEM simulation results in Fig. 6a-c show that, under the same pressure conditions, the piezoelectric potential increases with increasing the number of micropores in ZnO. This increase in piezoelectric potential is related to larger densities of atoms closer to the surface that can experience greater deformation under stress because of fewer bonding neighbors in contrast to bulk atoms [51,52]. This effect leads to improved polarization of surface atoms that are responsible for enhancing piezoelectric properties, which explains why our porous ZnO can generate higher piezoelectric potential compared to commercial ZnO, which lacks this high density of surface sites.

ZnO is an n-type semiconductor with an inherent limitation for piezoelectric applications due to its abundance of free carriers caused by internal defects and impurity atoms. These free carriers weaken the piezo-potential output due to the potential screening effect schematically depicted in Fig. 6d [53–55]. To mitigate this issue, we introduced AgNWs into porous ZnO with the intention of creating a 3D electrically conductive path to reduce internal resistance and enhance free carrier flow. Under the influence of non-electrostatic forces, free carriers easily migrate to the AgNWs and are then transferred to the electrode (Fig. 6e). This mechanism minimizes sacrificing positive charges [56–58], which,

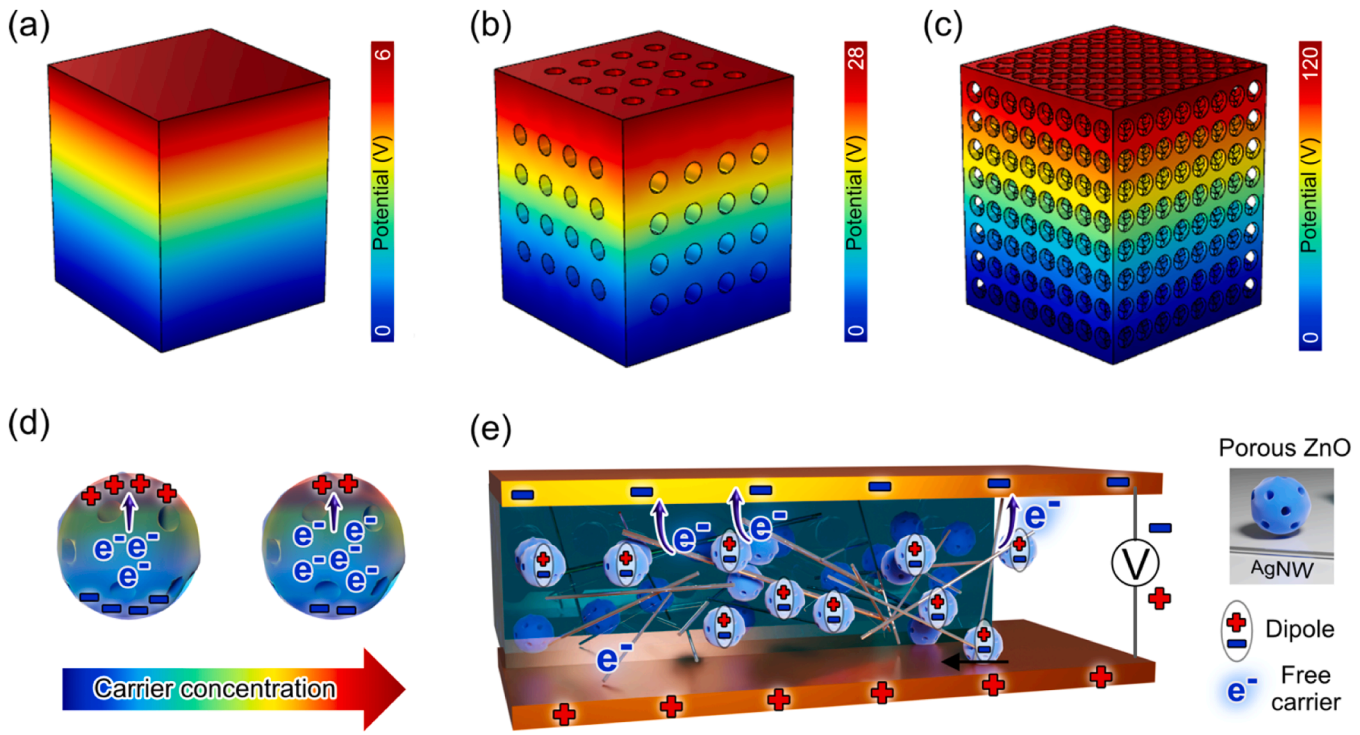

Fig. 6. (a) FEM simulation results for the electric potential in nonporous ZnO under uniform stress. (b) and (c) Show the potential in commercial and porous ZnO, respectively, with the porous structure enhancing the piezoelectric response. (d) Illustration of how increasing free carrier concentration affects the piezoelectric potential. (e) Mechanistic view of the piezoelectric process within the ZnO-AgNWs/PDMS PTNG.

in turn, significantly enhances the piezoelectric voltage generated.

One more consequence of introducing AgNWs to our composite material is the enhancement of triboelectric properties via boosting surface charge density and the improvement of relative capacitance [59–61]. We verified this triboelectric output performance enhancement by results presented in Figs. 2d and 2e. The superior performance observed for the final composite is partly attributed to enhanced electron transfer across the triboelectric layers, making a more effective charge distribution.

3. Conclusions

For the first time, we showed the development and evaluation of high-performance piezo-triboelectric nanogenerators using porous ZnO as the piezoelectric material, AgNWs as the conductive filler, and PDMS as the triboelectric flexible polymer matrix. This synergistic combination advances sustainable energy harvesting and self-powered wearable electronics with ultra-robust and long-term performance. Moreover, we created this hybrid material using conventional electrospinning, sintering, molding, and curing. These methods are widely available in material science and easy to implement elsewhere, contributing to replicating the findings reported here.

Here below, we summarize five key properties and characteristics that our rational design with this unique combination of materials allows:

1. **Electric output**: We showed impressive electrical output metrics, generating an open-circuit voltage of 146 V and a short-circuit current of 1.1 μA@12.5 kPa thanks to the synergistic effect of the piezoelectric properties of porous ZnO and the triboelectric effect of the PDMS polymer enhanced by AgNWs.
2. **Flexibility and wearability**: The flexibility of our PTNG makes it ideal for integration into wearable devices undergoing 300 % stretching and various kinds of deformations without reliability issues.
3. **Long-term stability**: Over 60 days with no performance degradation. This is crucial for real-world applications that require reliability over extended periods.
4. **Energy harvesting**: Our device converts mechanical energy from everyday movements into electrical energy and power wearables as illustrated by the energy generated from regular walking.
5. **Sensing**: In addition to energy harvesting, the PTNG device performs as a sensor responding to external pressure with high sensitivity.

4. Experimental

4.1. Materials

Zinc acetate ($C_4H_6OZn•2H_2O$; Aladdin), PDMS (Beijing Sanjing Faith New Materials Technology Co., Ltd.), Zinc oxide (Liben-Rubber Trading Co., Ltd), $AgNO_3$ (Chengdu Kelong Chemical Co., Ltd.), ethylene glycol (EG; Chengdu Kelong Chemical Co., Ltd.), poly(N-vinylpyrrolidone) (PVP, Mw≈1300,000; Chengdu Kelong Chemical Co., Ltd.), NaCl (Chengdu Kelong Chemical Co., Ltd.), NaBr (Chengdu Kelong Chemical Co., Ltd.), $Fe(NO_3)_3$ (Chengdu Kelong Chemical Co., Ltd.), and $FeCl_3•6H_2O$ (Chengdu Kelong Chemical Co., Ltd.) were used in the experiment. All chemical reagents were of analytical reagent grade, and the deionized water had a conductivity of less than 0.055 μS/cm.

4.2. Preparation of porous ZnO

As shown in Figures S1a and S1b, porous ZnO was prepared by electrospinning followed by high-temperature sintering. First, PVP/ethanol solution with a concentration of 0.001 M was obtained by adding PVP into ethanol with magnetic stirring at 60 ℃ until PVP was completely dissolved. Then, the precursor solution was prepared by adding 0.8 g of zinc acetate and 1 mL of deionized water into 10 mL PVP/ ethanol solution while stirring until the solution was colorless and transparent. Next, the precursor solution was loaded into a syringe connected with a 16 kV DC power supply, and precursor fibers were

prepared by electrospinning at a flow rate of 1 mL/h. Finally, the precursor fibers were dried in an oven at 60 ℃ for 2 h and calcined at 700 ℃ for 5 h in the air atmosphere to obtain porous ZnO.

4.3. Synthesis of silver nanowires

AgNWs were prepared by the low-temperature hydrothermal synthesis technology [62]. PVP dissolved in EG with a concentration of 0.15 M was first prepared before three kinds of mediated agents (NaCl, NaBr, and Fe $(NO_3)_3$) were added to the solution. Then, a solution of $AgNO_3$/EG with a concentration of 0.1 M was also prepared by dissolving $AgNO_3$ in EG. Later on, the above two solutions were mixed at a volume ratio of 1:1 under ultrasonic treatment for 10 min to ensure uniformity. Afterward, the mixture was poured into a Teflon-lined stainless-steel autoclave and kept at 160 ℃ for 3 h. Finally, AgNWs were obtained after being rinsed three times with absolute alcohol.

4.4. Preparation of ZnO-AgNWs/PDMS PTNG

The as-prepared porous ZnO was mixed with AgNWs and PDMS to obtain a slurry (Figure S1c), which was then drop-coated on a substrate (Figure S1d). A flexible composite was eventually obtained after being cured under vacuum conditions for 5 h (Figure S1e). The ZnO-AgNWs/PDMS PTNG was finally achieved by using copper foil as electrodes. In a similar way, three other PTNGs were fabricated based on pure PDMS, commercial ZnO powders with PDMS, and the porous ZnO with PDMS for comparison, which were defined as PDMS PTNG, commercial ZnO/PDMS PTNG, and ZnO/PDMS PTNG, respectively.

4.5. Characterization

The morphologies of the samples were observed by scanning electron microscopy (SEM, Helios G4 UC, Thermo Fisher Scientific) equipped with energy-dispersive X-ray analysis (EDX, Aztec Live ULTIM, Oxford Instruments). Information on the phase of the as-prepared porous ZnO was obtained by X-ray powder diffraction measured on a SmartLab-9 kW diffractometer (XRD, Rigaku, Japan) using Cu Kα radiation (λ = 0.15418 nm) under 40 kV and 30 mA, within a scanning range from 20° to 80° at step intervals of 0.02°. The adsorption-desorption curve and micropore size distribution spectrum were measured by Micromeritics ASAP 2460 3.00 BET surface area analyzer using nitrogen as absorbent at −195.8 ℃.

4.6. Device assembly and electrical characterization

All the composite films were cut to a sample size of 1 × 2 cm^2. Nitrile rubber was used as the contact material for electrical output testing. In the hybrid electrical output testing, copper foil electrodes were attached to both sides of the sample. The copper foil on one side was the same size as the sample, whereas on the other side, it was half the size. Specifically, the single-electrode testing method was employed to evaluate the triboelectric response, with the copper foil electrode affixed to only one side of the device. In contrast, for piezoelectric output testing, copper electrodes matching the size of the device were attached to its opposite sides. Cyclic compressive pressure was used for electrical output testing, with a magnitude of 12.5 k Pa. The open-circuit voltages were measured with a digital oscilloscope (Rigol, DS1102Z-E, China), and the short-circuit currents were measured with an electrochemical workstation (Chenhua, CHI660E, China). The quasi-static test method was employed to measure the piezoelectric coefficient of both the commercial ZnO/PDMS composite and the porous ZnO/PDMS composite using a d_{33} meter (Sinocera, YE2730A, China).

CRediT authorship contribution statement

Chen Jin-Ju: Supervision, Conceptualization. **Zhao Sheng-Zhe:** Methodology. **Chen Wei:** Writing – review & editing, Writing – original draft, Resources, Methodology, Formal analysis, Data curation. **Lu Ran:** Methodology, Conceptualization. **Xiang Guo-Tao:** Visualization. **Rodriguez Prof. Dr. Raul D.:** Writing – review & editing, Visualization. **Xu Jia-Lei:** Data curation. **Hu Yong-Da:** Writing – review & editing. **Sheremet Evgeniya:** Formal analysis.

Declaration of Competing Interest

The authors declare that they have no known competing financial interests or personal relationships that could have appeared to influence the work reported in this paper.

Acknowledgements

The work was supported by the Sichuan Science and Technology Program (grant No. 2023YFG0215) and the Chengdu Science and Technology Program (grant No. 2023-GH02-00021-HZ). R. D. R. and E. S. acknowledge funding from Russian Science Foundation grant No. 22-12-20027, https://rscf.ru/project/22–12-20027/ and the funding from Tomsk Region Administration.

Appendix A. Supporting information

Supplementary data associated with this article can be found in the online version at doi:10.1016/j.sna.2025.116264.

Data Availability

Data will be made available on request.

References

[1] Y.Y. Mao, Y. Li, J.Y. Xie, H. Liu, C.J. Guo, W.B. Hu, Nano Energy 84 (2021) 105918.
[2] W.K. Lin, B. Wang, G.X. Peng, Y. Shan, H. Hu, Z.B. Yang, Adv. Sci. 8 (2021) 2002817.
[3] R. Li, Z.Y. Xu, L. Li, J.J. Wei, W.Q. Wang, Z.J. Yan, T. Chen, Chem. Eng. J. 454 (2023) 140261.
[4] Y.Y. Mao, L. Liu, M.C. Xu, J.Y. Xie, W.B. Hu, Nano Energy 125 (2024) 109609.
[5] L. Liu, Y.T. Li, M.C. Xu, R. Tao, Q. Zhong, X. Yang, S.X. Lan, J.Y. Xie, G. Chen, Y. Y. Mao, W.B. Hu, Chem. Eng. J. 474 (2023) 145866.
[6] M.Q. Li, B.G. Xu, Z.H. Li, Y.Y. Gao, Y.J. Yang, X.X. Huang, Chem. Eng. J. 450 (2022) 137491.
[7] X.X. Li, D.X. Ji, B.X. Yu, R. Ghosh, J.H. He, X.H. Qin, S. Ramakrishna, Chem. Eng. J. 426 (2021) 130345.
[8] N. Wang, C.Z. Gao, F. Xue, Y. Han, T. Li, X. Cao, X.J. Zhang, Y. Zhang, Z.L. Wang, ACS Nano 9 (2015) 3159.
[9] Y.J. Su, C.X. Chen, H. Pan, Y. Yang, G.R. Chen, X. Zhao, W.X. Li, Q.C. Gong, G. Z. Xie, Y.H. Zhou, S.L. Zhang, H.L. Tai, Y.D. Jiang, J. Chen, Adv. Funct. Mater. 31 (2021) 2010962.
[10] D.Y. Park, J.J. Daniel, D.H. Kim, H. Park, J.H. Han, C.K. Jeong, H. Park, J.G. Park, B. Joung, K.J. Lee, Adv. Mater. 29 (2017) 1702308.
[11] M. Anithkumar, A.P.S. Prasanna, N.R. Alluri, S.J. Kim, Adv. Funct. Mater. 33 (2023) 2303562.
[12] H.H. Singh, N. Khare, Nano Energy 51 (2018) 216.
[13] C. Rodrigues, A. Gomes, A. Ghosh, A. Pereira, J. Ventura, Nano Energy 62 (2019) 660.
[14] X.X. Chen, M.D. Han, H.T. Chen, X.L. Cheng, Y. Song, Z.M. Su, Y.G. Jiang, H. X. Zhang, Nanoscale 9 (2017) 1263.
[15] K.Y. Lee, M.K. Gupta, S.W. Kim, Nano Energy 14 (2015) 139.
[16] J.L. Li, J.Y. Cai, J.Y. Yu, Z.L. Li, B. Ding, Adv. Funct. Mater. 33 (2023) 2303249.
[17] Z.L. Wang, J.H. Song, Science 312 (2006) 242.
[18] A.T. Le, M. Ahmadipour, S.Y. Pung, J. Alloy. Compd. 844 (2020) 156172.
[19] Y.Z. Du, C.K. Fu, Y.Z. Gao, L. Liu, Y.W. Liu, L.X. Xing, F. Zhao, RSC Adv. 7 (2017) 21452.
[20] D. Tamvakos, S. Lepadatu, V.A. Antohe, A. Tamvakos, M. Weaver, L. Piraux, M. G. Cain, D. Pullini, Appl. Surf. Sci. 356 (2015) 1214.
[21] Z.M. Zhang, Y. Ning, X.S. Fang, J. Mater. Chem. C 7 (2019) 223.
[22] G.L. Mantini, Y.F. Gao, A. D'Amico, C. Falconi, Z.L. Wang, Nano Res. 2 (2009) 624.
[23] D.C. Yang, Y. Qiu, Q.Y. Jiang, Z.S. Guo, W.B. Song, J. Xu, Y. Zong, Q.X. Feng, X. L. Sun, Appl. Phys. Lett. 110 (2017) 063901.
[24] Y.T. Changa, J.Y. Chena, T.P. Yang, C.W. Huang, C.H. Chiu, P.H. Yeh, W.W. Wu, Nano Energy 8 (2014) 291.
[25] L.S. Kang, H.L. Ana, J.Y. Park, M.H. Hong, S. Nahm, C.G. Lee, Appl. Surf. Sci. 475 (2019) 969.

[26] S. Lee, J. Lee, W. Ko, S.N. Cha, J.I. Sohn, J.M. Kim, J.G. Park, Y.J. Park, J.P. Hong, Nanoscale 5 (2013) 9609.
[27] T.T. Pham, K.Y. Lee, J.H. Lee, J.H. Lee, K.H. Kim, K.S. Shin, M.K. Gupta, B. Kumar, S.W. Kim, Energy Environ. Sci. 6 (2013) 841.
[28] Y. Hu, L. Lin, Y. Zhang, Z.L. Wang, Adv. Mater. 24 (2012) 110.
[29] G. Tian, D. Xiong, Y.H. Su, T. Yang, Y.Y. Gao, C. Yan, W. Deng, L. Jin, H.T. Zhang, X.Q. Fan, C.M. Wang, W.L. Deng, W.Q. Yang, Nano Lett. 20 (2020) 4270.
[30] S.N. Lu, J.J. Qi, Y.S. Gu, S. Liu, Q.K. Xu, Z.Z. Wang, Q.J. Liang, Y. Zhang, Nanoscale 7 (2015) 4461.
[31] Y.F. Gao, Z.L. Wang, Nano Lett. 9 (2009) 284.
[32] R. Pandey, V. Singh, P.I. Anand, P.I. Anand, S.J. Kim, ACS Appl. Mater. Interfaces 11 (2019) 6078.
[33] Y. Zhu, B. Yang, J. Liu, X.Z. Wang, L.X. Wang, X. Chen, C.S. Yang, Sci. Rep. 6 (2016) 22233.
[34] H. Wang, M. Shi, K. Zhu, Z.M. Su, X.L. Cheng, Y. Song, X.X. Chen, Z.Q. Liao, M. Zhang, H.X. Zhang, Nanoscale 8 (2016) 18489.
[35] Y. Yang, H. Tian, H. Sun, R.J. Xu, Y. Shu, T.L. Ren, RSC Adv. 4 (2014) 2115.
[36] H. Sun, H. Tian, Y. Yang, D. Xie, Y.C. Zhang, X. Liu, S. Ma, H.M. Zhao, T.L. Ren, Nanoscale 5 (2013) 6117.
[37] B. Dudem, D.H. Kim, L.K. Bharat, J.S. Yu, Appl. Energ. 230 (2018) 865.
[38] Y.K. Du, P. Yang, Z.G. Mou, N.P. Hua, L. Jiang, J. Appl. Polym. Sci. 99 (2006) 26.
[39] X. Peng, K. Dong, C.Y. Ye, Y. Jiang, Z.L. Wang, Sci. Adv. 6 (2020) 9624.
[40] S. Cao, H. Zou, B. Jiang, M. Li, Q. Yuan, Nano Energy 102 (2022) 107635.
[41] J.L. Zhang, T. Yang, G. Tian, B.L. Lan, W.L. Deng, L.H. Tang, Y. Ao, Y. Sun, W. H. Zeng, X.R. Ren, Z.Y. Li, L. Jin, W.Q. Yang, Adv. Fiber Mater. 6 (2023) 133.
[42] Q.T. Zhu, X.Y. Song, X.F. Chen, D.D. Li, X. Tang, J.B. Chen, Q.Q. Yuan, Nano Energy 127 (2024) 109741.
[43] X.Y. Song, B. Zhuo, S.A. Cao, L.J. Huang, Q.T. Zhu, J.Y. Zhang, Q.Q. Yuan, Appl. Surf. Sci. 649 (2024) 158996.
[44] Q. Chen, Y.Y. Cao, Y. Lu, W. Akram, S. Ren, L. Niu, Z. Sun, J. Fang, ACS Appl. Mater. Interfaces 16 (2024) 6239–6249.
[45] G.G. Xabier, A. Ghaffarinejad, F.J. Aparicio, C.S. Javier, L.S. Carmen, J.P. Espinós, J. Cotrino, R.S.V. Juan, A. Barranco, A. Borras, Nano Energy 91 (2022) 106673.
[46] Y.J. Fu, J.H. Liu, J.Y. Zou, S.J. Xu, Y.H. Wei, W. Zhang, D.W. Li, Chem. Eng. J. 489 (2024) 151495.
[47] R. Sasikumar, B. Kim, R.M. Bhattarai, Chem. Eng. J. 491 (2024) 151889.
[48] J.C. Li, J. Yin, M. Gui, V. Wee, A. Chinnappan, S. Ramakrishna, Adv. Fiber Mater. 5 (2023) 1417–1430.
[49] M. Mariello, L. Fachechi, F. Guido, M. Vittorio, D. Conformal, Adv. Funct. Mater. 31 (27) (2021) 2101047.
[50] Y. Lei, J. Yang, Y. Xiong, S. Wu, W.G.-S. Guo, Q. Sun, Z.L. Wang, Chem. Eng. J. 462 (2023) 142170.
[51] S.X. Dai, M. Gharbi, P. Sharma, H.S. Park, J. Appl. Phys. 110 (2011) 104305.
[52] R.C. Cammarata, Prog. Surf. Sci. 46 (1994) 1.
[53] D.C. Yang, Y. Qiu, Q.Y. Jiang, Z.S. Guo, W.B. Song, J. Xu, Y. Zong, Q.X. Feng, X. L. Sun, Appl. Phys. Lett. 110 (2017) 063901.
[54] Y.H. Sun, X.Q. Yan, Zheng, X. Zheng, Y. Li, Y.C. Liu, Y.W. Shen, Y. Ding, Y. Zhang, Nano Res. 10 (2017) 77.
[55] Lu, S.N. Lu, Q.L. Liao, J.J. Qi, S. Liu, Y.C. Liu, Q.J. Liang, G.J. Zhang, Y. Zhang, Nano Res. 9 (2016) 372.
[56] Z. Zhang, Q.L. Liao, Y.H. Yu, X.D. Wang, Y. Zhang, Nano Energy 9 (2014) 237.
[57] J. Briscoe, M. Stewart, M. Vopson, C.S.K. Ranasinghe, A. Yamakata, T. Nagai, K. J. Kimoto, Y.C. Kobayashi, N. Tamai, T.T. Affiliation, Adv. Energy Mater. 2 (2012) 1261.
[58] Y. Zhang, Y. Liu, Z.L. Wang, Adv. Mater. 23 (2011) 3004.
[59] J. Zhang, Y.L. He, C. Boyer, K.K. Zadeh, S.H. Peng, D.W. Chu, C.H. Wang, Nanoscale Adv. 3 (2021) 5465.
[60] Z.Q. Liu, M. Muhammad, L. Cheng, E.Q. Xie, W.H. Han, Appl. Phys. Lett. 117 (2020) 143903.
[61] X.M. He, H.Y. Guo, X.L. Yue, J. Gao, Y. Xi, C.U. Hu, Nanoscale 7 (2015) 1896.
[62] X.M. Wang, L. Chen, Enrico Sowade, R.D. Rodriguez, E. Sheremet, C.M. Yu, R. R. Baumann, J.J. Chen, Nanomaterials 10 (2020) 237.

Wei Chen is a postgraduate student at the School of Materials and Energy, University of Electronic Science and Technology of China. His research direction primarily focuses on the development of energy conversion devices and energy storage devices.

She-Zhe Zhao is a postdoctoral fellow at the School of Materials and Energy, University of Electronic Science and Technology of China. His research interests mainly focus on the development and performance study of nanomaterials.

Guo-Tao Xiang is currently working toward a doctoral degree at the School of Materials and Energy, University of Electronic Science and Technology of China. His research focuses on the fabrication and application of nanomaterials and structures in the field of environmental energy conversion and storage devices.

Ran Lu joined the School of Materials and Energy, University of Electronic Science and Technology of China to pursue a master's degree in 2020. His main research interest is the development of flexible energy storage devices.

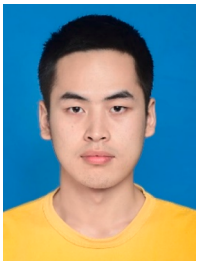

Jia-Lei Xu is a postgraduate student at the School of Materials and Energy, University of Electronic Science and Technology of China. His research interest mainly focuses on the synthesis and application of nano silver materials.

Professor Raul D. Rodriguez has a strong track record in nanoscience and nanotechnology. He obtained his Ph.D. with the highest honors from Pierre-Marie Curie (Sorbonne) University in Paris, France 2009. Prof. Rodriguez specializes in nanoscale characterization and has significantly contributed to developing innovative methods. Currently, he holds the position of Full Professor at Tomsk Polytechnic University. He leads research on flexible electronics with laser processing, including exploring plasmonic and 2D nanomaterials for cutting-edge applications in biomedicine, optoelectronics, energy, and safety.

Dr. Evgeniya Sheremet has been a Professor at the Research School of Chemical and Biomedical Sciences at Tomsk Polytechnic University, Russia, since 2017. Her academic journey began with studying Nanotechnology at Novosibirsk State Technical University. In 2015, she earned her Ph.D. in Experimental Physics from the Chemnitz University of Technology, where she focused her thesis on "Micro- and nano-Raman characterization of organic and inorganic materials." Following her doctorate, Prof. Sheremet continued her research in nanocharacterization as part of the Solid Surfaces Analysis group at TU Chemnitz. Her work involved employing finite element simulations of the electromagnetic field. Currently, she collaborates with Prof. Rodriguez to lead the dynamic research group TERS-Team. Their primary focus is exploring nanomaterials, their modification, analysis, and applications.

Yong-Da Hu is currently an associate professor at the School of Integrated Circuit Science and Engineering, University of Electronic Science and Technology of China. His current research focuses on vacuum thin film technology and sensor components.

Jin-Ju Chen is currently a professor at the School of Materials and Energy, University of Electronic Science and Technology of China. She received her doctoral degree in Microelectronics and Solid State Electronics from the University of Electronic Science and Technology of China in 2006, and worked as a visiting scholar at the Chemnitz University of Technology in Germany from 2015 to 2016. Her current research focuses on flexible wearable materials for sensors, energy nanogenerators and energy storage devices.